

N 7 3 3 2 6 1 4

NASA TM X-71431

**NASA TECHNICAL
MEMORANDUM**

NASA TM X-71431

**CASL FILE
COPY**

**THE EFFECTS OF INLET TEMPERATURE AND PRESSURE
DISTORTION ON TURBOJET PERFORMANCE**

by Willis M. Braithwaite, Edwin J. Graber, Jr., and Charles M. Mehalic
Lewis Research Center
Cleveland, Ohio

TECHNICAL PAPER proposed for presentation at Ninth Propulsion Joint Specialists
Conference sponsored by the American Institute of Aeronautics and Astronautics
and the Society of Automotive Engineers
Las Vegas, Nevada, November 5-7, 1973

THE EFFECT OF INLET TEMPERATURE AND PRESSURE DISTORTION ON TURBOJET PERFORMANCE

Willis M. Braithwaite, Edwin J. Graber, Jr.
and Charles M. Mehalic
Lewis Research Center
National Aeronautics and Space Administration
Cleveland, Ohio

Abstract

The effects on stability of steady-state, 180 degree extent circumferential distortions of inlet total temperature and pressure were experimentally determined for a turbojet engine. Results for both individual and combined temperature and pressure distortions are presented showing the losses incurred in stall pressure ratio and are compared with results predicted using a simplified parallel compressor model. The loss due to combined distortions was dependent upon the relative orientation between the low pressure and high temperature regions. Reasonable agreement was achieved between the predicted and observed loss in stall pressure ratio when based on a constant corrected speed relationship.

Introduction

A persistent problem in the development of air breathing propulsion systems for new aircraft is the uncertainty of the detrimental effect of non-uniform inlet flow on engine stability. These flow distortions often result from: aircraft maneuvers; the unforeseen coupling of the inlet and engine; and hot gas ingestion resulting from armament firing, recirculation of exhaust gases in STOL-VTOL applications, or wakes from other aircraft.

Considerable experimental effort has been expended to develop an understanding of the effects of pressure distortions. A relatively small effort has been made to understand temperature distortions, reference 1 to 9. Typically, these were either investigations of steam ingestion resulting from catapult launches of aircraft or missile exhaust gas ingestion.

An experimental program to further the understanding of the effects of inlet flow distortions on engine performance has been undertaken and is continuing at the NASA Lewis Research Center. Part of this program, which is reported herein, was to compare the effects of pressure and temperature distortion, separately and in combination, on the performance of an aircraft engine. To simplify this investigation, a simple turbojet engine, a J85-GE-13, was tested in an altitude facility. This engine has a single-spool eight-stage axial flow compressor with variable inlet guide vanes (IGV) and third, fourth and fifth stage bleeds that are scheduled as a function of corrected rotor speed.

The results presented in this paper have been restricted to those obtained with

circumferential one-per-revolution 180° extent distortions. The effects on engine performance of varying the circumferential and radial extent of inlet pressure distortions were also investigated and are reported in reference 10. The results herein are restricted to corrected rotor speeds from 90 to 100 percent where the bleeds were closed and the inlet guide vanes fixed. Also, only data obtained at one Reynolds number index, 0.67, is reported. The inlet total pressure and temperature on the undistorted side of the engine was maintained at approximately 2/3 of an atmosphere and 21°C, respectively.

The results are presented and discussed in four sections. The first covers the distortion of inlet total pressure; the second discusses temperature distortion; combined distortion is discussed third; and finally, the results are compared with those predicted using a simplified parallel compressor model. The combined pressure and temperature distortion data includes the effects of varying the relative position of the low pressure and high temperature regions.

Results and Discussion

The effect of engine inlet total pressure and temperature distortions, individually and in combination, on compressor stability limits are presented in terms of stall pressure ratio loss. The instrumentation used for the analysis of the distortions is briefly discussed. Finally, a simplified parallel compressor model is used to predict the effect of the distortions on stability limits and comparisons are made with experimentally determined results.

Total Pressure Distortion

Compressor inlet total pressure distortion was generated by placing screens of varying solidity in the inlet duct approximately one diameter upstream of the engine inlet. The orientation of the screens relative to the six inlet total pressure rakes of five elements each is shown in figure 1. Also shown in figure 1 is the location of the compressor exit instrumentation comprised of four rakes of four total pressures and one total temperature each. The distortion screens blocked a 180° sector of the inlet annulus extending from 90° clockwise to 270°, figure 1.

Typical circumferential profiles resulting from averaging the pressures on each rake are shown in figure 2. The total pressure profile at the compressor inlet reasonably approximates a 180° extent square wave whereas the

static pressure profile appears sinusoidal. While not presented, the radial variation of total pressure was approximately that of an undistorted inlet. The compressor exit profiles, figure 2, show very little circumferential variation in either total or static pressure, however, a total temperature distortion is evident. If it is assumed that the region of higher exit temperature is the result of the higher heat of compression in the distorted sector, then the distorted flow rotated approximately 90° in the direction of rotor rotation in passing from the low pressure sector of the compressor inlet to the compressor exit.

The total pressure distortion parameter used in this paper is defined as

$$\Delta P/P = (P_{ud} - P_d) / P_{av} \quad (1)$$

where P_d is the average of the pressure measurements on the two rakes behind the distortion screen, figure 1. P_{ud} is defined as the average of the pressure measurements on the two rakes in the undistorted region. P_{av} is the average of P_d and P_{ud} . A complete list of symbols is included at the end of the paper.

The effect of increasing the distortion amplitude (screen solidity) on the compressor stall line is shown on the undistorted compressor map, figure 3. Each stall line is defined as the locus of stall points generated for each screen used. Each stall point was generated by closing the exhaust nozzle while holding the mechanical speed of the rotor constant. Increasing the amplitude of the pressure distortion caused the stall line to move to lower pressure ratios. Also, the corrected rotor speed lines shift to the left or to lower airflows as shown in figure 3 for 93 percent corrected speed. The pressure distortion for a given screen as defined by equation 1 is not constant with airflow. As can be seen in figure 3 for screen "A" the pressure distortion varied from 5 percent at 90 percent speed to 12 percent at rated speed.

The parameter ΔPRS , describing the loss in stall pressure ratio, is used to evaluate the effects of flow distortion. Two variations of this parameter are considered depending on whether the difference in stall pressure ratio is evaluated at constant corrected airflow or at constant corrected speed. The two definitions are:

$$(\Delta PRS)_w = 1 - PRS_e / PRS_b \quad (2)$$

$$(PRS)_N = 1 - PRS_e / PRS_c \quad (3)$$

where PRS_e refers to the stall pressure ratio observed with distortion, figure 3, PRS_b is

the clean inlet stall pressure ratio at the same corrected airflow and PRS_c is the stall pressure ratio at the same corrected rotor speed as the observed stall point. Each definition has its use and we are not advocating one over the other. $(\Delta PRS)_w$ is a useful parameter for engine-inlet matching whereas $(\Delta PRS)_N$ is easier to evaluate in that it does not require an accurate measurement of engine airflow. It is also more compatible with the parallel compressor model as will be discussed later.

The effect of increasing the total pressure distortion on $(\Delta PRS)_w$ is shown in figure 4. A definite effect of corrected rotor speed is observed. The relationship between $(\Delta PRS)_w$ and $\Delta P/P$ is represented by a separate curve for each value of corrected speed. The ratio of $(\Delta PRS)_w$ to $\Delta P/P$ is seen to vary from 0.50 to 1.0 over the range of corrected speeds and amplitudes shown. Only at 93 percent corrected speed was the ratio constant with amplitude.

In contrast, $(\Delta PRS)_N$, figure 5, is essentially linear with $\Delta P/P$ and the effect of speed is insignificant. The ratio of $(\Delta PRS)_N$ to $\Delta P/P$ is approximately 0.60. Again, only the data for speeds above 90 percent are presented inasmuch as this is the region where the bleeds are closed and the IGV are in a fixed position.

The results of the pressure distortion phase of the investigation can be summarized as follows. A circumferential distortion of inlet total pressure was accompanied by a distortion of inlet static pressure and compressor exit total temperature. There was no distortion observed in exit static or total pressure. Increasing the amplitude of the total pressure distortion lowered the stall line and shifted the corrected speed lines to lower corrected flows. The reduction in stall pressure ratio based on a constant corrected speed definition of ΔPRS , ratioed to the amplitude of the pressure distortion was 0.60. Using a constant corrected airflow definition for ΔPRS resulted in a considerable scatter in the data due to a speed effect.

Temperature Distortion

The total temperature of the air entering the lower half of the compressor annulus was heated by a gaseous hydrogen burner. The design and construction of this burner is described in reference 4. Briefly, gaseous hydrogen was burned in the 180° sector of the burner located upstream of the inlet duct bellmouth approximately four diameters ahead of the engine inlet. The hydrogen flow was regulated to provide the desired temperature rise in the heated sector.

The instrumentation used for the temperature and the combined pressure and temperature distortion data, figure 6, differed from that shown in figure 1. There were 12 rakes of 5 thermocouples each at the compressor inlet. One rake of two total pressure measurements was located near the center of each 90° inlet sector. The total pressure elements at the

compressor exit were reduced from four to one per rake and the total temperature elements were increased from one to three per rake.

The rake average circumferential profiles of compressor inlet and exit total pressure and temperature are presented in figure 7. The effective number of measurements used to construct the profiles was increased by rotating the heated 180° sector in 90° steps and combining the four resultant profiles into the ones presented. The inlet temperature profile was more sinusoidal than the desired square wave pattern. Also, the temperature distortion persisted through the compressor with only a 29 percent reduction in the maximum amplitude, while the total pressure distortion, figure 2, was completely attenuated at the compressor exit. Comparison of the compressor inlet and exit total temperature profiles indicate the peak temperature distortion rotated approximately 45° in the direction of rotor rotation. There was little or no circumferential distortion of total or static pressure associated with the temperature distortion at the compressor inlet or exit.

The temperature distortion parameter used in this paper is defined as:

$$\Delta T/T = (T_d - T_{ud}) / T_{av} \quad (4)$$

T_d is the average of all 30 temperature measurements in the heated region, T_{ud} is the average of the remaining temperature measurements and T_{av} is the average of all 60 measurements.

The effects on the stall line of increasing the temperature distortion level are presented on the undistorted compressor map of figure 8. The distorted stall line is defined as the locus of stall points for a constant distortion amplitude. Increasing the temperature distortion decreased the stall pressure ratio. Another effect was the decrease in corrected rotor speed for a constant mechanical speed. The constant corrected speed lines also moved to lower values of corrected airflow as shown in the figure for 92 percent corrected speed.

The loss in stall pressure ratio evaluated at constant corrected airflow is shown in figure 9 and appears to be nearly linear with the amplitude of the temperature distortion. The ratio of $(\Delta PRS)_w$ to $\Delta T/T$ is approximately 0.75.

The loss in stall pressure ratio at constant corrected speed, figure 10, also appears to be linear. Here, the ratio of $(\Delta PRS)_N$ to $\Delta T/T$ is approximately 0.62. There is an indication of a second order effect of corrected rotor speed as the higher speed points are slightly lower than the lower speed points. This effect is more noticeable on $(\Delta PRS)_N$ than for the constant airflow case.

The results of the temperature distortion phase of the investigation can be summarized as follows. The effects of increasing the

the amplitude of the temperature distortion was to shift the constant corrected speed lines to the left on the compressor map and to reduce the stall pressure ratio. The loss in stall pressure ratio was approximately a constant ratio of 0.75 and 0.62 of the distortion amplitude based on $(\Delta PRS)_w$ and $(\Delta PRS)_N$, respectively. There appeared to be essentially no effect of variations in corrected rotor speed on ΔPRS . The temperature distortion passed through the compressor with only a 29 percent reduction in amplitude and the distorted sector rotated approximately 45° in the direction of rotor rotation.

Combined Pressure and Temperature Distortion

The effect on the stall pressure ratio of combined inlet pressure and temperature distortion was investigated by placing an 180° circumferential extent screen between the gaseous hydrogen burner and the compressor inlet. Only one screen was used during the investigation and it covered the top half of the inlet throughout this phase of the investigation. The effect of varying the position of the low pressure sector relative to the heated sector was evaluated by rotating the heated sector through four circumferential positions. The first position of the 180° extent temperature distorted sector coincided with the location of the 180° extent pressure distortion. The resulting circumferential profiles of inlet total pressure and temperature are shown in figure 11a. The pressure profiles noted in the figure are from figure 2 inasmuch as the pressure instrumentation at the compressor inlet was meager and temperature distortion alone (figure 7) caused no pressure distortion.

The second position of the temperature distorted sector was rotated 90° from the first, figure 11b. Thus one 90° quadrant of the inlet had both a higher temperature and lower pressure than average, the second quadrant had a higher temperature and pressure than average, the third quadrant had a higher pressure and lower temperature than average and the fourth quadrant had a lower pressure and temperature than average. For the third position, the temperature distortion was rotated another 90° and coincided with the region of maximum pressure, figure 11c. For the fourth position, the temperature distortion was again rotated 90° placing it on the opposite side of the inlet from that noted in figure 11b.

The four positions of the temperature distortion had different effects on the stall points as shown in figure 12. The pressure distortion for all configurations varied from about 9 percent at 93 percent speed to about 12 percent at 99 percent speed. The temperature distortion was approximately 7 percent. The opposed pressure and temperature distortion had little effect on the stall line. The two overlapped configurations, which produced similar effects, had a greater effect on the stall line, 7 percent $(\Delta PRS)_N$ and the coincident pattern had the most severe effect, 9 percent $(\Delta PRS)_N$ at 96 percent corrected rotor

speed. The loss in stall pressure ratio for the superimposed distortion is about the same as it would have been for pure pressure distortion. However, the temperature distortion had reduced the average corrected rotor speed by approximately 3 1/2 percent before the comparison was made. Thus, for the same 180° extent distortion in inlet pressure and temperature, but differently oriented, the loss in stall pressure ratio varied from near zero for the opposed pattern to approximately 9% for the superimposed distortions. It is, therefore, possible to reduce the effect of the pressure distortion by creating an opposed temperature distortion. However, there could be a loss in performance resulting from the lower corrected rotor speed.

Parallel Compressor Model

An understanding of the effects on the compressor stall limits of inlet distortions may be enhanced by the use of a simple parallel compressor model. This approach is similar to that used by other investigators, reference 11. The basic assumptions and methods used in applying this model will be presented followed by a comparison of the loss in stall pressure ratio predicted by the model with those obtained experimentally. Finally, a few simplifying assumptions will be made to allow one to make comparison between the theory and some of the distortion indicators used today.

Parallel Compressor Theory

The basic assumptions used in the model presented herein are listed in figure 13. The distorted compressor is, for analytical purposes, assumed to consist of a set of parallel compressors (hereafter called sub-compressors), each operating independently of the others. All of these sub-compressors are assumed to have individually uniform inlet flow conditions and to have the same performance characteristics as the undistorted compressor. No cross-flow is permitted between these sub-compressors throughout their length, but the streamlines may swirl and thereby allow the distortion pattern to rotate from its inlet orientation. Since all the sub-compressors discharge into a common plenum, their exit static pressures are assumed identical. The entire compressor is assumed to be in stall when the pressure ratio of any sub-compressor equals the stall pressure ratio.

An additional assumption was made based on the experimental results for the J-85 turbojet engine. The compressor exit total pressure was found to be uniform, figures 2 and 7, and was, therefore, assumed to be identical for all the sub-compressors. This assumption is the only non-standard one used in the parallel compressor model used herein and was made only to simplify the calculation procedure. In the general case with non-uniform exit total pressure, an additional map would be required similar to the normal performance map but with a compressor exit static-to-inlet total pressure ratio being used instead of the normal

total-to-total pressure ratio.

Application of the Model

The method by which the model was applied to the various distortions investigated is shown schematically in figure 14. As the amplitude of a simple 180° total pressure distortion is increased, the operating point of the distorted inlet sub-compressor (No. 1, fig. 14a) will move to higher pressure ratios along the constant speed characteristic until the stall line is reached. Whereas the undistorted sub-compressor (2 on figure 14a) is assumed to remain at the same operating point. As mentioned previously, the overall compressor is considered to be in stall when any sub-compressor's pressure ratio equals the stall pressure ratio. The resultant overall compressor stall pressure ratio (pt. s) is then defined as the ratio of the common exit total pressure to the average inlet total pressures of all the sub-compressors. The overall corrected airflow is defined as the sum of all the individual sub-compressor airflows corrected to the average of the inlet total pressures and temperatures.

Increasing the inlet temperature of the distorted sub-compressor moves its operating point horizontally (fig. 14b) at constant compressor pressure ratio since the inlet total pressures as well as exit total pressures are identical for all the sub-compressors with only temperature distorted inlet flow. This pressure ratio is also the overall stall pressure ratio. The overall corrected airflow is found in the same manner as before.

The four cases of combined 180° total pressure and temperature distortions are shown in figures 14c and 14d. Since only 180° temperature distortions, 180° pressure distortions, and combinations of these resulting in either 0°, 90° or 180° of overlap are considered in this report, the compressor was divided into four sub-compressors, each with an inlet pressure and temperature equal to the quadrant average value. In the case of the 90° and 180° overlap, the operating point of the quadrant with the distorted temperature (high) and pressure (low) will reach the stall line as the amplitude of either, or both, distortion is increased. Thus the critical pressure ratio is determined. In the case of the 0° overlap (opposed) pressure and temperature distortion, the pressure ratio of either sub-compressor could be critical. Therefore, two separate solutions are made, first assuming the pressure distorted sub-compressor pressure ratio was critical, and, secondly, considering the temperature distorted sub-compressor to be critical. An overall compressor stall pressure ratio is determined as the ratio of the common exit total pressure to the average of the sub-compressor inlet total pressures. The exit total pressure is obtained by multiplying the critical pressure ratio by the sub-compressor inlet total pressure. The corrected airflow is determined as before as the sum of the individual quadrant airflows corrected to the compressor average inlet total pressure and temperature. The loss in stall pressure

ratios are determined by equations 2 and 3.

Comparison with Data

The experimentally determined values of ΔPRS are compared with analytically predicted values based on the parallel compressor model, figures 15 and 16. Relatively good agreement with theory in terms of $(\Delta PRS)_N$ is indicated in figure 15. The scatter is not considered excessive in that a one percent difference in $(\Delta PRS)_N$ can result from an .08 percent difference in pressure ratio.

On a constant airflow basis, figure 16, the trend is about the same but the increased scatter is probably the result of the inaccuracies associated with the measured airflows, and, to a lesser degree, to the uncertainties of the clean inlet compressor map which was determined by a relatively few experimental data points.

Simplified Model

In an effort to develop a direct mathematical relationship between $(\Delta PRS)_N$ and $\Delta P/P$ and $\Delta T/T$ which is more amenable to hand calculations, an additional simplification was added. Based on experimental data from 90 to 100 percent speed, the stall pressure ratio was expressed as a linear function of the corrected speed.

$$PR = A(N/\sqrt{\theta}) + B \quad (5)$$

It is also noted that at stall:

$$P_3 = (PR)_K (P_{2,K}) \quad (6)$$

where $(PR)_K$ is the pressure ratio for the sub-compressor in which stall originates and $P_{2,K}$ is the inlet pressure of this sub-compressor. Combining equations 5, 6 and 3 results in

$$(\Delta PRS)_N = 1 - \left(\frac{P_{2,K}}{P_{2,av}} \right) \frac{A(N/\sqrt{\theta_K}) + B}{A(N/\sqrt{\theta_{av}}) + B} \quad (7)$$

Consider now the combined temperature and pressure distortion patterns shown in figures 14c and 14d. A stall can originate in one of the sub-compressors where:

- 1, $P_K = P_d$ and $T_K = T_{ud}$ as for the opposed, fig. 14c
- 2, $P_K = P_{ud}$ and $T_K = T_d$ as an alternate solution for the opposed distortions, fig. 14c.
- 3, $P_K = P_d$ and $T_K = T_d$ as for the overlapped distortions of figure 14d.

The average pressure and temperature are given by

$$P_{av} = (P_{ud} - P_d) \left(1 - \frac{\theta_P}{2\pi} \right) + P_d \quad (8)$$

$$T_{av} = (T_d - T_{ud}) \left(\frac{\theta_T}{2\pi} \right) + T_d \quad (9)$$

The subscripts d and ud refer to the average values of pressures and temperatures of the sub-compressor inlets as defined previously. θ_P is the angular extent of the minimum pressure sub-inlet and θ_T is the angular extent of the maximum temperature sub-inlet.

For the sub-compressor number one, equation 7 combined with equations 8 and 9, becomes

$$(\Delta PRS)_N = 1 - \frac{1 - \frac{\Delta P}{P} \left(1 - \frac{\theta_P}{2\pi} \right)}{1 + \frac{B}{A(N/\sqrt{\theta_{av}})}} \left[\left(1 - \frac{\Delta T}{T} \frac{\theta_T}{2\pi} \right)^{-\frac{1}{2}} + \frac{B}{A(N/\sqrt{\theta_{av}})} \right] \quad (10)$$

For sub-compressor number two,

$$(\Delta PRS)_N = 1 - \frac{1 + \frac{\Delta P}{P} \left(\frac{\theta_P}{2\pi} \right)}{1 + \frac{B}{A(N/\sqrt{\theta_{av}})}} \left[\left\{ 1 + \frac{\Delta T}{T} \left(1 - \frac{\theta_T}{2\pi} \right) \right\}^{-\frac{1}{2}} + \frac{B}{A(N/\sqrt{\theta_{av}})} \right] \quad (11)$$

and for sub-compressor number three,

$$(\Delta PRS)_N = 1 - \frac{1 - \frac{\Delta P}{P} \left(1 - \frac{\theta_P}{2\pi} \right)}{1 + \frac{B}{A(N/\sqrt{\theta_{av}})}} \left[\left\{ 1 + \frac{\Delta T}{T} \left(1 - \frac{\theta_T}{2\pi} \right) \right\}^{-\frac{1}{2}} + \frac{B}{A(N/\sqrt{\theta_{av}})} \right] \quad (12)$$

The critical sub-compressor is the one with the largest value of $(\Delta PRS)_N$. For the overlapping distortion this is always sub-compressor number three and equation 12 is used to determine $(\Delta PRS)_N$. For the opposed distortions, $(\Delta PRS)_N$ is the largest of those given by equations 10 and 11. The separate cases of only pressure distortion or only temperature distortion are obtained by setting $\Delta T/T$ or $\Delta P/P$ respectively equal to zero.

For small values of $\Delta P/P$ and $\Delta T/T$, a further simplification can be made by expanding the terms involving $\Delta T/T$ in a binomial expansion and neglecting second and higher order terms such as $(\Delta T/T)^2$, $(\Delta P/P)^2$ and $(\Delta T/T)(\Delta P/P)$. The resulting equations are respectively

$$(\Delta PRS)_N = \frac{\Delta P}{P} \left(1 - \frac{\Theta_P}{2\pi}\right) - \frac{1}{2} \frac{\Delta T}{T} \left(\frac{\Theta_T}{2\pi}\right) \left/ \left(1 + \frac{B}{A(N\sqrt{\Theta_{av}})}\right) \right. \quad (10a)$$

$$(\Delta PRS)_N = -\frac{\Delta P}{P} \left(\frac{\Theta_P}{2\pi}\right) + \frac{1}{2} \frac{\Delta T}{T} \left(1 - \frac{\Theta_T}{2\pi}\right) \left/ \left(1 + \frac{B}{A(N\sqrt{\Theta_{av}})}\right) \right. \quad (11a)$$

$$(\Delta PRS)_N = \frac{\Delta P}{P} \left(1 - \frac{\Theta_P}{2\pi}\right) + \frac{1}{2} \frac{\Delta T}{T} \left(1 - \frac{\Theta_T}{2\pi}\right) \left/ \left(1 + \frac{B}{A(N\sqrt{\Theta_{av}})}\right) \right. \quad (12a)$$

A parametric plot of the above equations is shown in figure 17 for a corrected speed of 97 percent. For $\Delta P/P = 0$, the linear relationship shown here of $(\Delta PRS)_N = 0.73 \Delta T/T$ compares favorably with that of figure 10, $(\Delta PRS)_N = 0.625 \Delta T/T$. With $\Delta T/T = 0$, the model yields $(\Delta PRS)_N = 0.5 \Delta P/P$ as compared to the experimental value of $0.6 \Delta P/P$, fig. 5.

The importance of the relative location of the combined pressure and temperature distortions should be noted. Referring to figure 17, if a 12 percent low pressure region of 180° extent coincides with a 14 percent high temperature region of 180° extent, $(\Delta PRS)_N$ is found to be about 16 percent. If, however, the distortions are placed opposite one another, $(\Delta PRS)_N$ is approximately 4 percent with stall originating in the high inlet temperature sub-compressor. Thus, a dramatic difference in the value of $(\Delta PRS)_N$ results from the relative position of the distorted pressure and temperature regions.

The simplified model also predicts the same $(\Delta PRS)_N$ for both the 90° and 180° overlapping distortions, figure 17. This is in agreement with the concept of reference 12 that there is little effect of the circumferential extent of a distortion above some minimum. However, the experimental results, figure 12, indicate that the 180° overlap drops the stall pressure ratio more than the 90° overlapping distortions. This may be due to the lack of a

proper shape factor in determining $\Delta P/P$ and especially $\Delta T/T$ inasmuch as they are not true square wave patterns as assumed for the model.

Summary of Results

An investigation into the effects of 180° extent inlet distortion of total pressure and temperature, both individually and in combination, was conducted using a J85-GE-13 turbojet engine. The loss in stall pressure ratio (ΔPRS) was compared with that predicted by a parallel compressor model. The results obtained are as follows:

1. With inlet pressure distortion alone, the ratio of $(\Delta PRS)_N$ to the amplitude of the distortion, $\Delta P/P$, was approximately 0.60 and was essentially independent of speed. The ratio of $(\Delta PRS)_w$ to $\Delta P/P$, however, varied with speed and amplitude from values of 0.50 to 1.0. The distortion in inlet total and static pressure was completely attenuated in passing through the compressor. However, a distortion in total temperature resulted at the compressor exit, rotated 90° from the distorted inlet sector.

2. For inlet temperature distortion alone, ΔPRS was approximately a constant ratio of the distortion amplitude $\Delta T/T$ of 0.75 based on $(\Delta PRS)_w$ and 0.65 based on $(\Delta PRS)_N$. The temperature distortion was attenuated by approximately 29 percent in passing through the compressor and rotated approximately 45° from the distorted inlet sector. No distortion in total or static pressure was present at either the compressor inlet or exit.

3. The combined effect of pressure and temperature distortion on ΔPRS depended on the relative orientation between the distorted sectors. The ratio of $(\Delta PRS)_N$ to $\Delta P/P$ for a temperature distortion of 7 percent was approximately 0 when the distorted sectors were opposed to each other, 0.6 for the sectors overlapping, and 0.8 for the sectors superimposed.

4. The parallel compressor model predicted the effects of distortion on $(\Delta PRS)_N$ with better accuracy and with less scatter than $(\Delta PRS)_w$ over the range of conditions considered.

5. A simplified parallel compressor model was developed which closely correlated with the data and which graphically displayed the separate, combined and relative position effects of pressure and temperature distortion on $(\Delta PRS)_N$.

Symbols

- A slope of corrected rotor speed - stall pressure ratio line, $\Delta(PR) \div \Delta(N\sqrt{\Theta})$, equation 5.
- B Intercept of corrected rotor speed - stall pressure ratio line, equation 5.
- N Rotor speed, RPM

P Total pressure.
 P_s Static pressure.
 PRS Stall pressure ratio.
 ΔPRS Loss in stall pressure ratio, equations 2 and 3.
 S Average stall point, figure 14.
 T Total temperature.
 W Mass flowrate of air.
 δ Ratio of compressor inlet total pressure to standard ambient sea-level total pressure.
 θ Ratio of inlet total temperature to standard ambient sea-level total temperature.
 θ^* Circumferential position, degrees.
 θ_p Extent of pressure distortion, degrees.
 θ_T Extent of temperature distortion, degrees.

Subscripts:

a air
 av average, equations 1 and 4
 b,c,e pressure ratio noted on figure 3 and equations 2 and 3.
 d distorted sector (minimum pressure or maximum temperature side of inlet)
 K critical sub-compressor, equations 6 and 7
 max maximum
 min minimum
 N constant corrected rotor speed, eq. 3.
 r average of measurements on a rake
 ud undistorted sector (maximum pressure or minimum temperature side of inlet).
 W constant corrected airflow, equation 2.
 2 compressor inlet
 3 compressor exit

2. Wallner, L. E., Useller, J. W., and Saari, J., "A Study of Temperature Transients at the Inlet of a Turbojet Engine," RM E57C22, 1957, NACA, Cleveland, Ohio
3. Gabriel, L., Wallner, R., Lubick, R., and Vasu, G., "Some Effects of Inlet Pressure and Temperature Transients on Turbojet Engines," *Aeronautical Engineering Review*, Vol. 16, No. 9, Sept. 1957, pp. 54-59, 84.
4. Rudey, R. A., and Antl, R. J., "The Effect of Inlet Temperature Distortion on the Performance of a Turbo-Fan Engine Compressor System," Paper 70-625, June 1970, AIAA New York, N.Y.
5. Rich, W. A., and Reale, R. A., "J-52-P-6A Engine, Sea Level Missile Exhaust Gas Ingestion Tests," NAPTC-ATD-162, May 1969, Naval Air Propulsion Test Center, Trenton, N.J.
6. Rich, W. A., and Reale, R. A., "J-52-P-8A Engine Altitude Missile Exhaust Gas Ingestion Tests," NAPTC-ATD-195, Sept. 1969, Naval Air Propulsion Test Center, Trenton, N.J.
7. Rich, W. A., and Reale, R. A., "Specification Rocket Test for Turbojet/Turbofan Missile Gas Ingestion," NAPTC-ATD-197, Feb. 1971, Naval Air Propulsion Test Center, Trenton, N.J.
8. Felderman, E.J., and High, M.D., "Missile Exhaust Gas Ingestion Simulation," AEDC-TR-71-252, Dec. 1971, Aro, Inc., Arnold AF Station, Tenn.
9. Worobei, P., "Steam Ingestion Tests of a Pratt and Whitney Aircraft TF-30-P-8 Turbofan Engine," NAPTC-ATD-183, Nov. 1971, Naval Air Propulsion Test Center, Trenton, N.J.
10. Calogeras, J. E., Mehalic, C. M., and Burstadt, P. L., "Experimental Investigation of the Effect of Screen-Induced Total Pressure Distortion on Turbojet Stall Margin," TM X-2239, 1971, NASA, Cleveland, Ohio.
11. Melick, H. C., Jr., and Simpkin, W. E., "A Unified Theory of Inlet/Engine Compatibility," Paper 72-1115, Nov. 1972, AIAA New York, N.Y.
12. Reid, C., "The Response of Axial Flow Compressors to Intake Flow Distortion," Paper 69-GT-29, March 1969, ASME, New York, N.Y.

References

1. Childs, J. H., Kochendorfer, F. D., Lubick, R. J., and Friedman, R., "Stall and Flame-Out Resulting from Firing of Armament," RM E55E25, 1955, NACA, Cleveland, Ohio.

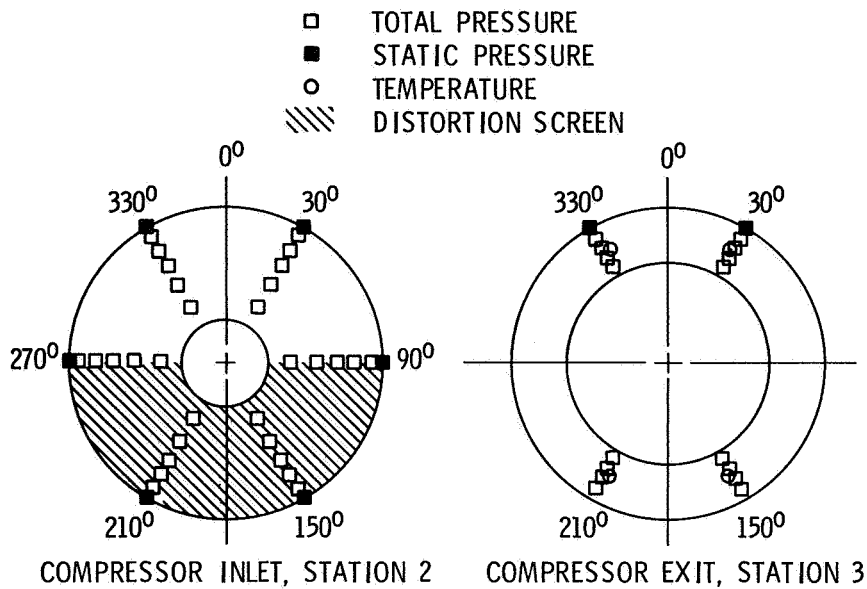


Figure 1. - Schematic of compressor instrumentation for pressure distortion tests. Viewed looking upstream.

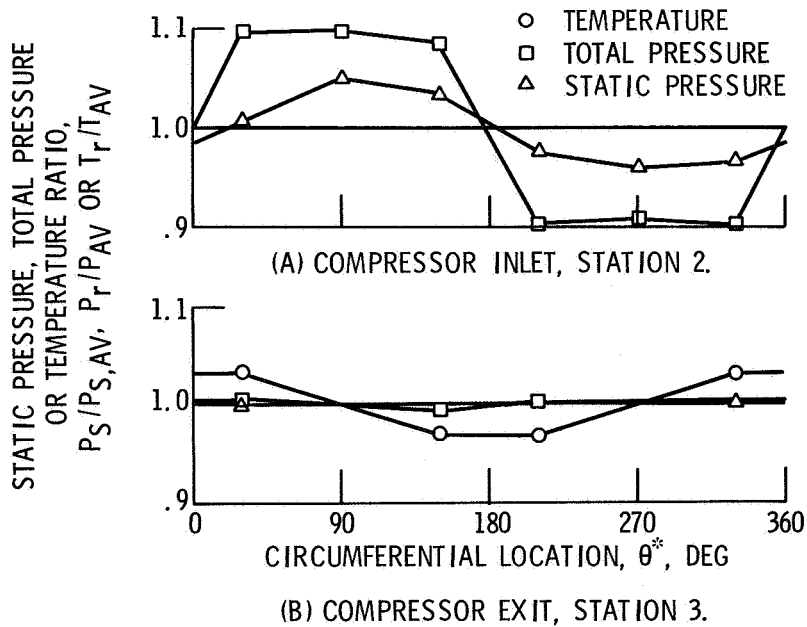


Figure 2. - Compressor profiles with 180° circumferential pressure distortion at 94 percent design speed.

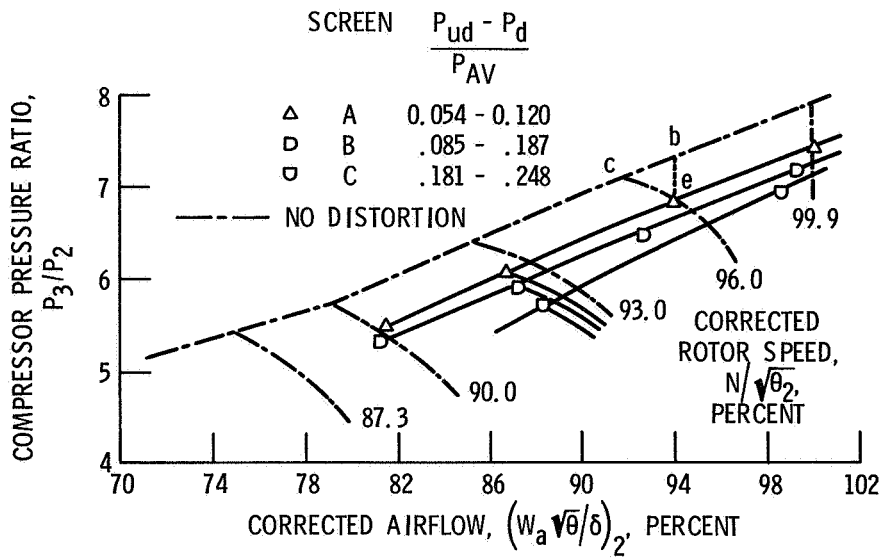


Figure 3. - Compressor map showing effects of 180° circumferential pressure distortion.

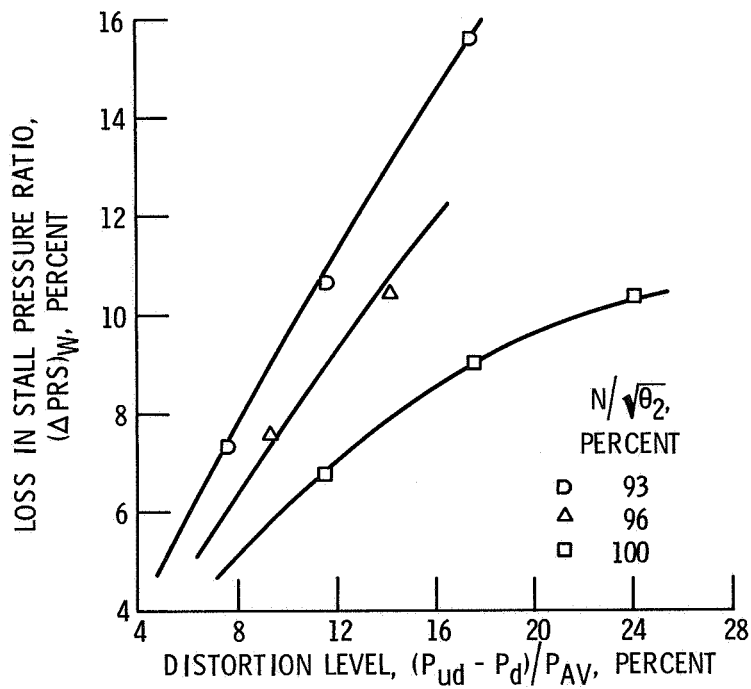


Figure 4. - Loss in stall pressure ratio at constant corrected airflow for 180° extent inlet pressure distortion.

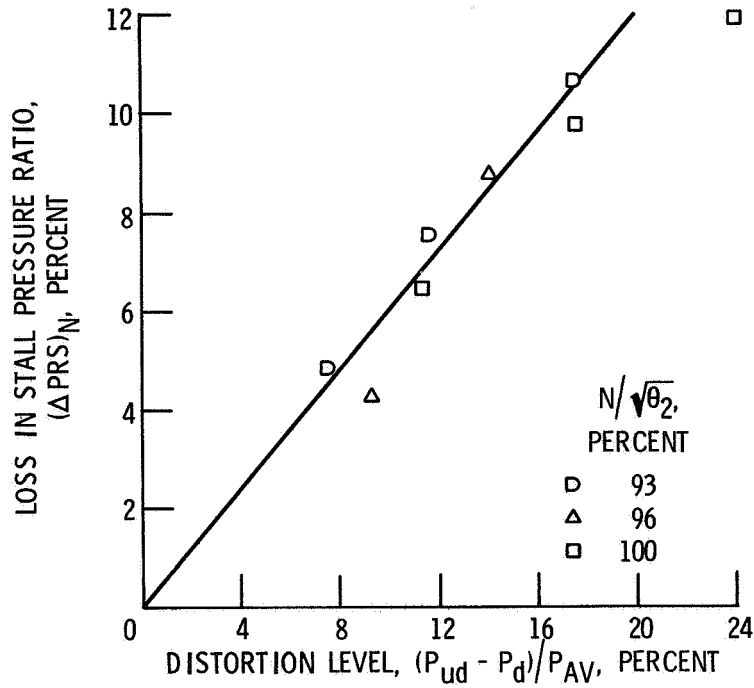


Figure 5. - Loss in stall pressure ratio at constant corrected speed for 180° extent inlet pressure distortion.

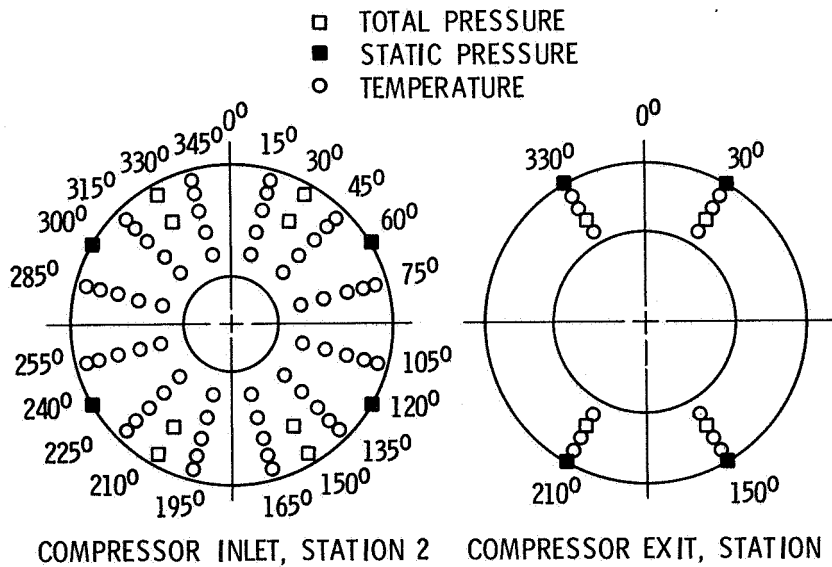


Figure 6. - Instrumentation schematic for temperature and combined temperature and pressure distortion tests as viewed looking upstream.

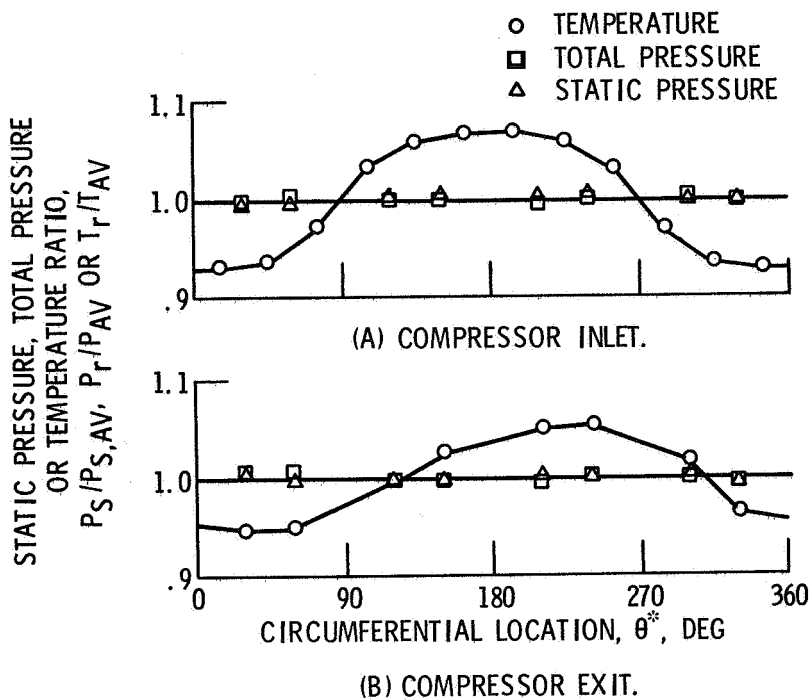


Figure 7. - Compressor profiles with 180° circumferential temperature distortion at 96 percent design speed.

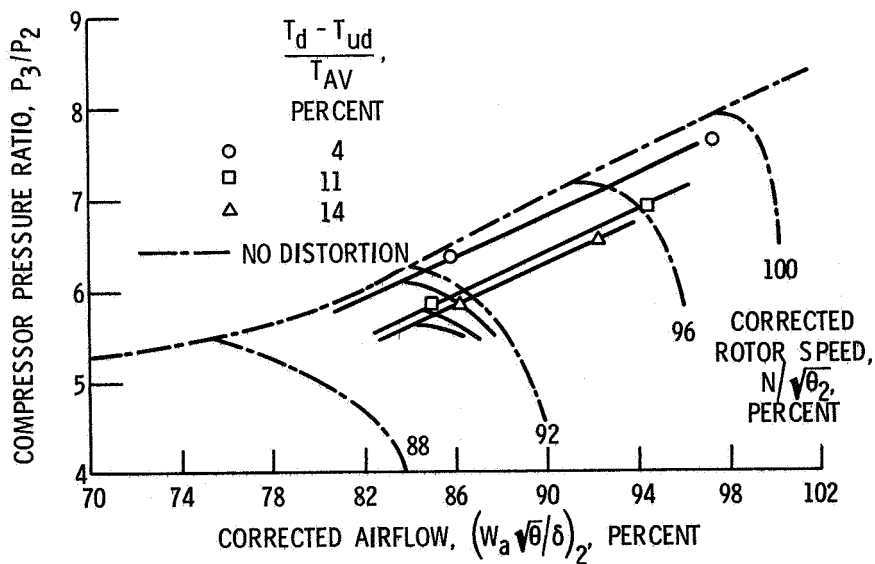


Figure 8. - Compressor map showing effects of 180° circumferential temperature distortion.

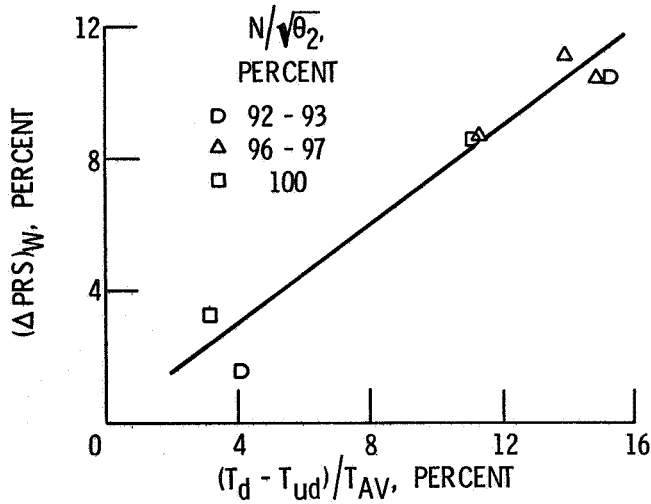


Figure 9. - Loss in stall pressure ratio at constant corrected airflow for 180° extent temperature distortion.

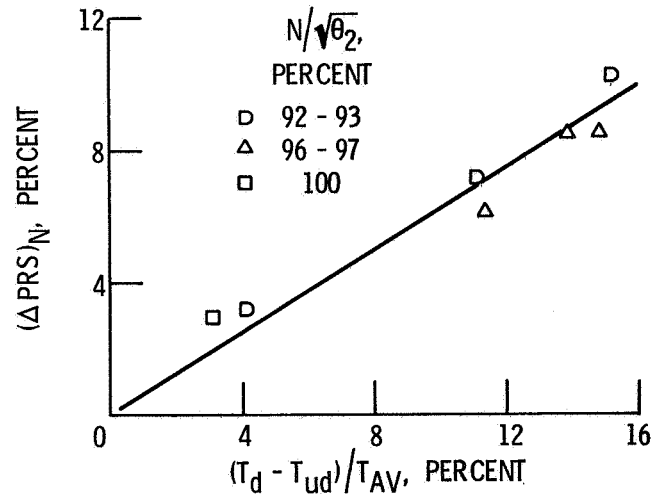


Figure 10. - Loss in stall pressure ratio at constant corrected speed for 180° extent temperature distortion.

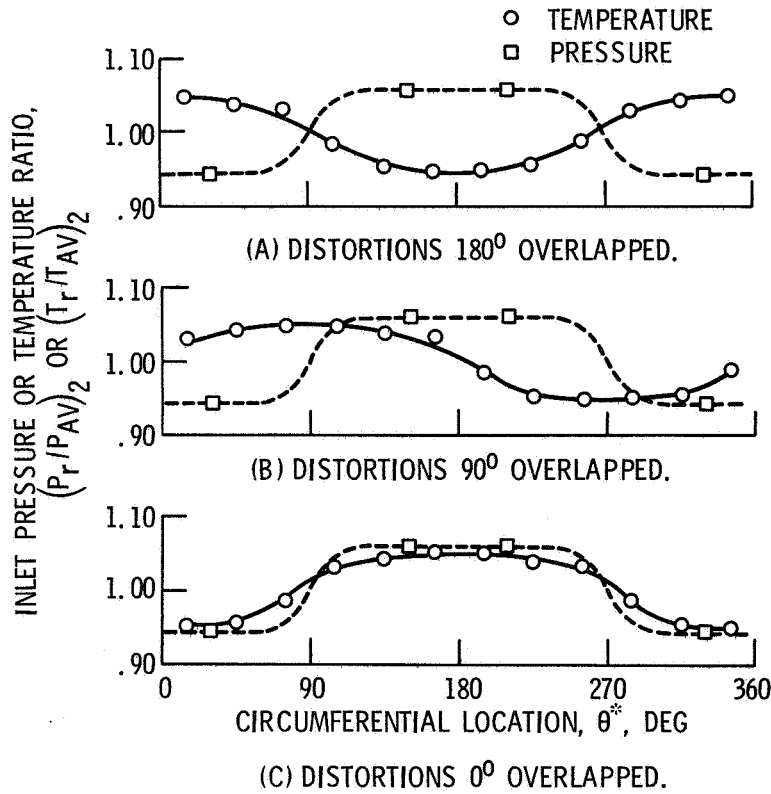


Figure 11. - Compressor inlet profiles with combined 180° extent pressure and temperature distortions.

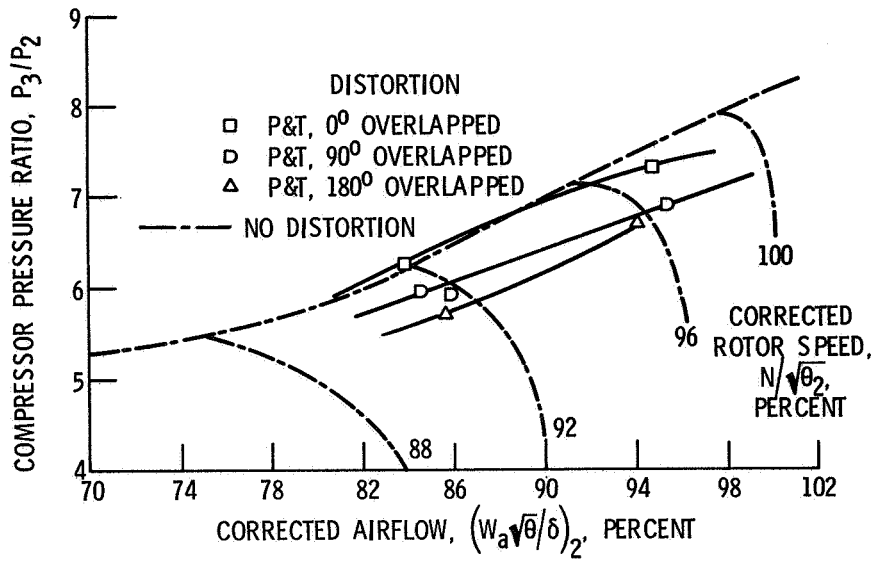
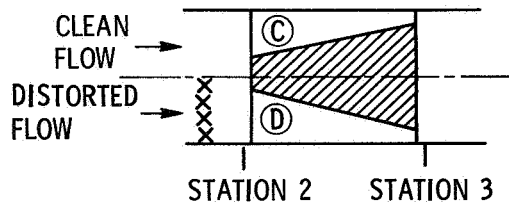


Figure 12. - Compressor map showing effects of 180° extent combined pressure and temperature distortion.



1. SECTORS C AND D ARE CONSIDERED AS INDEPENDENT PARALLEL COMPRESSORS
2. BOTH SECTORS FOLLOW SAME MAP AS UNDISTORTED COMPRESSOR
3. NO CROSSFLOW BETWEEN PARALLEL COMPRESSORS
4. BOTH EXIT TO A COMMON STATIC PRESSURE

Figure 13. - Assumptions used for parallel compressor model.

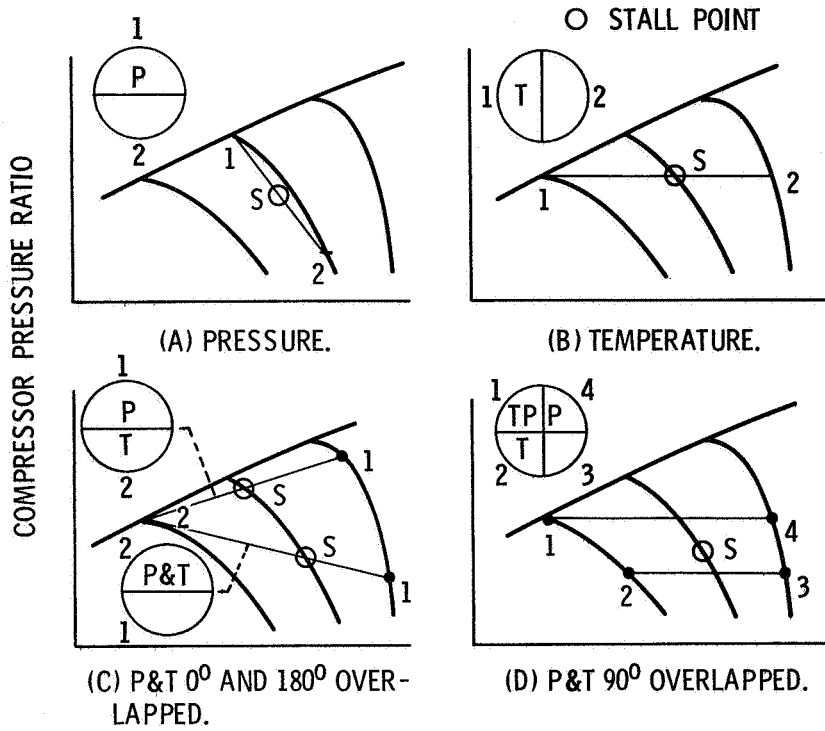


Figure 14. - Application of parallel compressor model.

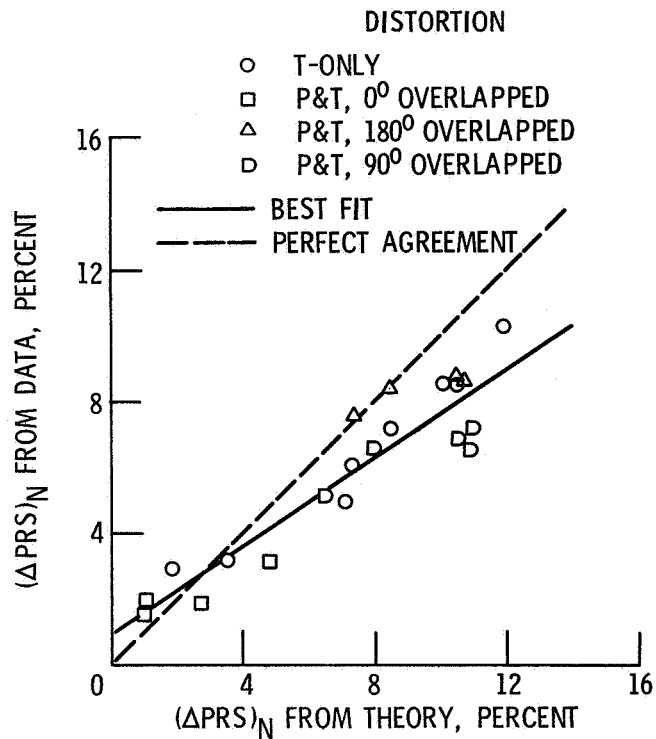


Figure 15. - Comparison between actual and predicted loss in stall pressure ratio using parallel compressor theory.

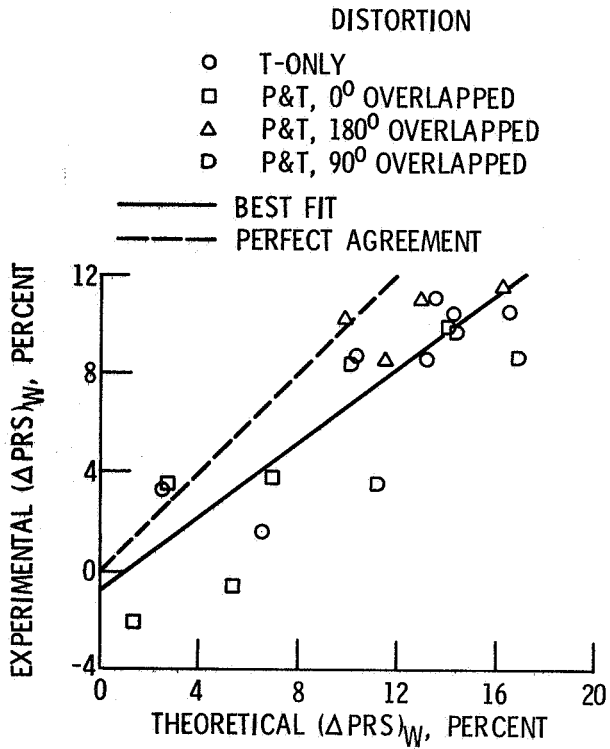


Figure 16. - Comparison between actual and predicted loss in stall pressure ratio using parallel compressor theory.

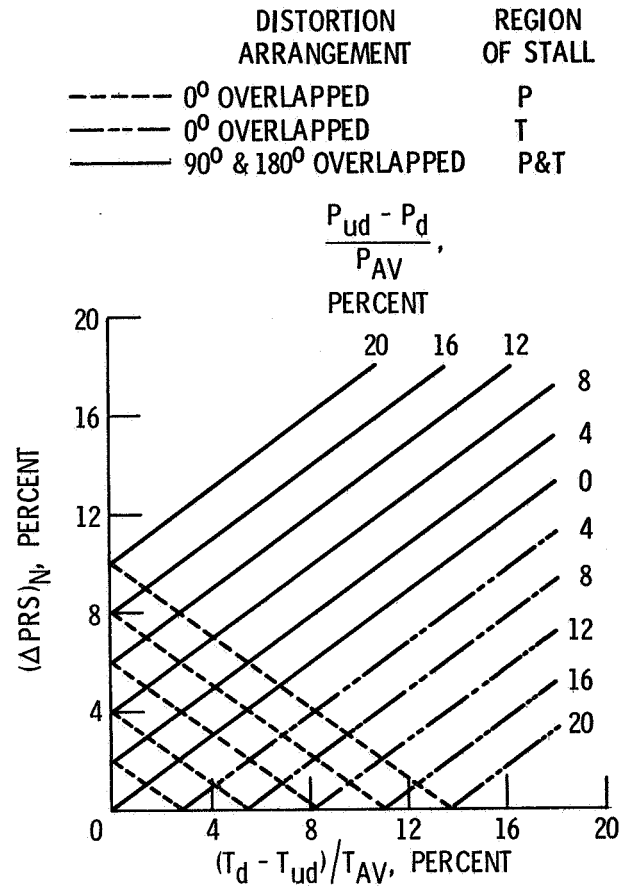


Figure 17. - Plot of simplified parallel compressor model for separate and combined 180° extent inlet pressure and temperature distortion for 97 percent corrected speed.